
Consideration of the Timing Effect of Dendrite Pinch-Off on Dendrite Fragmentation During Directional Solidification of Superalloys

Haijie Zhang ^a, Menghuai Wu ^{a*} and Abdellah Kharicha ^a

DOI: <https://doi.org/10.9734/bpi/mono/978-93-49473-95-9/CH2>

Peer-Review History:

This chapter was reviewed by following the Advanced Open Peer Review policy. This chapter was thoroughly checked to prevent plagiarism. As per editorial policy, a minimum of two peer-reviewers reviewed the manuscript. After review and revision of the manuscript, the Book Editor approved the manuscript for final publication. Peer review comments, comments of the editor(s), etc. are available here: <https://peerreviewarchive.com/review-history/3590.2>

ABSTRACT

Single-crystal superalloys play a vital role in aerospace and power generation due to their superior mechanical properties at high temperatures. However, the formation of freckles during the casting process is highly detrimental. The freckle is characterized by a trace of small misoriented spurious (equiaxed) grains with a local accumulation of eutectics. The primary source for the spurious grains is considered to be dendrite fragmentation. It is known that the interdendritic flow in the dendrite growth direction promotes dendrite remelting, creating favourable conditions for dendrite fragmentation. Therefore, a flow-driven fragmentation model was primarily proposed, assuming that the fragmentation occurs when the following criterion, $(\vec{u}_\ell - \vec{u}_c) \cdot \nabla c_\ell < 0$, is fulfilled. Although the above model has considered global transport phenomena and their impacts on the local thermodynamic condition for the dendrite remelting, some other microscopic events influencing the fragmentation were ignored or simplified. One such event is the timing effect of dendrite pinch-off. In this conference contribution, a modification to the previous flow-driven fragmentation model was suggested. In addition to the above flow-driven remelting criterion, a second condition, i.e., the necessary time for the remelting (t_r) of the dendrite roots to allow the pinch-off (τ) to occur, is applied to the model. An improved simulation-experiment agreement is achieved in terms of both the distribution of the segregation channel and the formation of spurious grains. The mechanisms for the onset of segregation channels and the production of spurious grains are studied.

^a Metallurgy Department, Chair of Simulation and Modelling Metallurgical Processes, Montanuniversitaet Leoben, Franz-Josef Street 18, 8700, Leoben, Austria.

*Corresponding author: E-mail: menghuai.wu@unileoben.ac.at;

Keywords: Solidification; dendrite fragmentation; timing effect; freckles; spurious grains.

2.1 INTRODUCTION

Nickel-based single-crystal superalloys play a vital role in aerospace and power generation due to their exceptional mechanical properties at high temperatures. The single-crystal growth is typically achieved through a grain selector (e.g. a spiral grain selector), through which only one crystal is expected. However, the formation of freckles in the subsequent solidification process destroys the integrity of the single-crystal casting. The freckle is characterized by a trace of mis-orientated small spurious grains and local enrichment of eutectics [1]. The formation mechanism for freckles has been well understood. The segregation of the solute elements in the mushy zone results in density inversion. In case of an upward solidification, the solute-enriched interdendritic liquid is less dense than the bulk liquid and thereby flows upward, which initiates the plumes and the formation of segregation channels beneath them [2]. The upward flow of solute-enriched liquid within the segregation channels eroded the roots of some higher-order dendrite arms, leading to dendrite fragmentation [3]. Eventually, the solute-enriched liquid solidifies as eutectics and the fragments solidify as spurious grains, which is termed as the freckle.

According to the engineering definition, freckles should be distinguished from segregation channels [1,4]. A segregation channel can be called a freckle only when it captures some spurious grains, while segregation channels without spurious grains can be at most called "quasi-freckles". However, in many previous works, the segregation channels were treated as freckles. In our recent work [5], it was found that a freckle is developed from a well-developed segregation channel. Fragments can only be produced when the upward flow in the segregation channel is sufficiently strong, and the local remelting conditions are sustained long enough to melt off the roots of higher-order side arms.

The mechanism behind freckle formation is well understood, but predicting and controlling these defects remains a challenging task. This difficulty arises from the complex geometry of blade castings and the intricate interactions between multiphase flow and solidification that occur during the directional solidification process. Despite the difficulties, advancements in numerical modelling offer potential solutions to bridge the gap between theoretical understanding and practical control. Recently, a digital-twin approach was proposed to model the solidification process [6]. Based on this approach, the formation of segregation channels was quantitatively predicted at the industrial scale of superalloy turbine blade casting. This digital twin approach was extended to involve dendrite fragmentation, and the previously proposed flow-driven fragmentation sub-model [7] was refined to consider the timing effect [5] to pinch off the roots of side arms. Details regarding the model description, experiment setups, and also validation of the numerical model refer to our previous works [5,8]. In this conference contribution, the main goal is to highlight the necessity of considering the timing effect in flow-driven fragmentation mechanisms for a quantitative prediction of the freckles.

2.2 MODEL CONFIGURATION AND DESCRIPTION OF THE CALCULATION METHOD

The directional solidification experiment was conducted in a Bridgman-type vacuum furnace. A cluster of superalloy specimens was assembled around the axis of the furnace. A spiral grain selector was used to achieve the single-crystal growth of the casting. The shell mould was preheated to 1750 K, after which it was filled with hot liquid metal at the same temperature. The composition of the studied superalloy is shown in Table 2.1. After a stabilization time of 10 min, the solidification was triggered by withdrawing the casting system downward from the hot chamber to the cold chamber at a speed of 1.5 mm/s. The selection of such a low casting speed is to provide a freckle-prone condition.

Table 2.1. Main composition of the superalloy

Elements	Ta	Cr	Al	Co	W	Re	Ti	Mo	Ni
Content (wt.%)	8.07	3.39	5.69	5.97	6.52	4.89	0.15	0.41	Balance

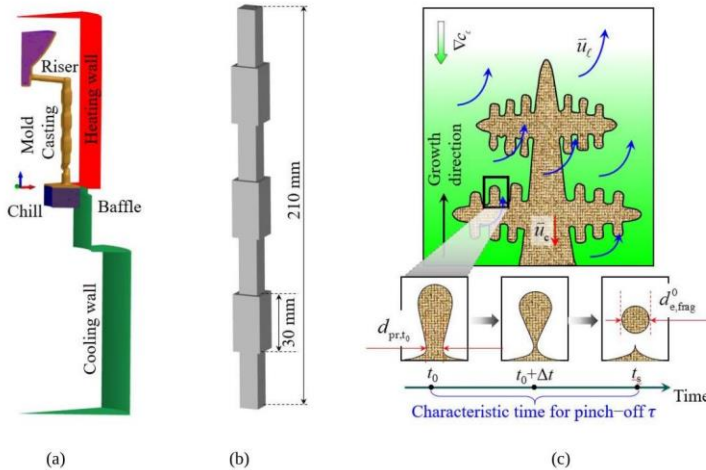


Fig. 2.1. Model configuration. (a) A layout of 1/12 of the Bridgman furnace and the casting system; (b) Casting shape and dimensions; (c) Schematic of the flow-driven fragmentation model and the timing of the pinch-off process of the side arm roots.

A full-scale geometry was built for the furnace and the casting system, and one-twelfth of the furnace is shown in Fig. 2.1(a). The geometry and dimension of the superalloy casting are presented in Fig. 2.1(b). The superalloy casting consists of seven segments with a square cross-section. The side length is 10 mm for the small square and 15 mm for the large square. Each segment is 30 mm high with a total height of the casting is 210 mm. In the current study, the previously proposed digital twin approach [6] was employed to model the freckle formation during the

directional solidification of a superalloy casting. The thermal calculation was conducted on the full-scale geometry, Fig. 2.1(a), using ProCAST, while the flow and solidification calculation was limited to the casting region, Fig. 2.1(b). Simulation settings and the relevant thermophysical material properties refer to previous papers [5,6].

The flow and solidification calculations were performed using the previously developed multiphase volume-average solidification model [9]. Three hydrodynamic phases, i.e., liquid, equiaxed, and columnar, are involved, with their volume fractions that sum to one, i.e., $f_\ell + f_e + f_c = 1$. Solidification and remelting are governed by diffusion, and thermodynamic equilibrium is applied at all solid-liquid interfaces. The columnar dendrites only originate from the bottom of the casting, and the equiaxed grains are solely produced via dendrite fragmentation. A flow-driven fragmentation sub-model has been proposed based on Flemings' theory [7]. As schematically demonstrated in Fig. 2.1(c), in case of an upward solidification, the solute concentration ∇c_ℓ increases with the mushy zone depth owing to the solute partition during the solidification process; The upward flow brings the interdendritic liquid with a higher solute concentration deep in the mushy zone to the tip region, which promotes remelting and thus dendrite fragmentation. On the basis of this, it was assumed the fragmentation event occurs when the criterion $(\vec{u}_\ell - \vec{u}_c) \cdot \nabla c_\ell < 0$ is fulfilled. This flow-driven fragmentation method has been successfully applied to steel [10] and Al-based alloys [11] to calculate the macrosegregation and microstructure. Nevertheless, it failed to calculate the formation of freckles during the directional solidification of superalloy castings.

There is no doubt that the liquid flow in the dendrite growth direction, i.e., $(\vec{u}_\ell - \vec{u}_c) \cdot \nabla c_\ell < 0$, promotes remelting. However, fragmentation cannot happen immediately when a remelting condition is fulfilled. As shown by the insets in Fig. 2.1(c), at t_0 , a side arm with a root diameter of d_{pr,t_0} undergoes a remelting condition, and the entire side arm starts to reduce in size. After a kinetic remelting process, e.g., at $t_0 + \Delta t$, the root part is pinched to a very thin rod. If the remelting condition is sustained, the root will be completely pinched off at t_s , that is, a fragment is produced. The time from t_0 to t_s is defined as the characteristic time τ for the pinch-off process, i.e., $\tau = t_s - t_0$. In our very recent work [5], a $t_r - \tau$ criterion was proposed to consider the timing of dendrite pinch-off for flow-driven fragmentation. t_r is the accumulative remelting time, which is recorded (i.e., $t_r = \sum_{i=1}^n \Delta t_i |(\vec{u}_\ell - \vec{u}_c) \cdot \nabla c_\ell < 0|$) during the calculation. Fragmentation occurs only when local accumulative remelting time is longer than the characteristic time for pinch-off, i.e., $t_r > \tau$. Details of the equations and more details can be found at [5].

2.3 SIMULATION RESULTS AND DISCUSSION

2.3.1 Solidification Sequence

The simulation results at 3800 s are depicted in Fig. 2.2. The calculated temperature field T on the casting surface is shown in Fig. 2.2(a). A mushy zone, with a maximal depth of about 35 mm, is formed between the top bulk liquid and the lower as-solidified casting. Owing to the shadow effect of the Bridgman

furnace, the casting facing the induction wall is much hotter than that facing the furnace axis. Hence, as displayed in Fig. 2.2(b), the solidification front is inclined. The solidification front is 9 mm higher on the shadowed side in comparison to the heating side. The solute partition on the liquid-solid interface leads to the continuous enrichment of the solute concentration c_ℓ with the mushy zone depth, Fig. 2.2(c). Both the solute expansion and thermal expansion modify the liquid density ρ_ℓ . From Fig. 2.2(d), it can be seen ρ_ℓ decreases with the casting height due to the increase of T , and decreases with the mushy zone depth due to the increase of c_ℓ , and the maximal ρ_ℓ is formed right above the solidification front. Such a density inversion drives the onset of plumes and the formation of segregation channels. The interdendritic liquid on the shadow side of the casting exhibits the highest gravitational potential, making it the most favourable location for the formation of plumes and segregation channels, which are illustrated in Fig. 2.2(e) by the yellow isosurfaces of $c_{\text{mix}}^{\text{index}} = 2.8\%$, with $c_{\text{mix}}^{\text{index}} = (c_{\text{mix}} - c_0)/c_0 \cdot 100\%$. Under the influences of thermal buoyancy, solutal buoyancy, and solidification-induced shrinkage, a complex flow pattern emerges. As shown in Fig. 2.2(e), the flow in the bulk liquid is primarily driven by thermal buoyancy. The relatively cooler liquid descends on the shadow side and rises on the hot side. In the upper half of the mushy zone, solute-enriched liquid with lower density flows upward along the segregation channels and plumes. In contrast, in the lower half of the mushy zone, the downward feeding flow induced by solidification shrinkage prevails, overwhelming the influence of solutal buoyancy. The downward feeding flow does not determine the initiation of segregation channels, but it has a significant effect on the further development of the as-formed segregation channels. According to our recent work [5], it was found that ignoring the shrinkage-induced feeding flow, the strength and shape of the segregation channels were overestimated.

2.3.2 Dendrite Fragmentation

Dendrite fragmentation and the formation of spurious grains are analyzed in Fig. 2.3. As mentioned in §2.2, in the current model, a fragment can be produced only when the two criteria are fulfilled, i.e., $t_r > \tau$ and $(\vec{u}_\ell - \vec{u}_c) \cdot \nabla c_\ell < 0$. The first criterion evaluates whether the local cumulative melting time is sufficiently long, and the second criterion determines whether the local flow conditions at the given moment meet the requirements for flow-driven remelting. The region marked in green in Fig. 2.3(a) indicates the location where the first criterion is satisfied, and the region marked in purple in Fig. 2.3(b) indicates the location where the second criterion is satisfied. Fragmentation will and can only occur in the overlapping regions of the green and purple areas. As depicted in Fig. 2.3(c), fragments are produced in the two segregation channels at the casting shadowed corners, and the maximal fragmentation rate is equal to $N_{\text{frag}} = 4.5 \times 10^7 \text{ m}^{-3} \text{ s}^{-1}$. The distribution of the number density of the formed spurious grains (n_e) is illustrated in Fig. 2.3(d). A large amount of spurious grains is formed in the as-developed segregation channel. Most of the grains were entrapped by the surrounding columnar phase immediately after their initiation. Some grains can float or sink in the channels, which can be seen in the zoom-in view of Fig. 2.3(d). Similar phenomena were observed by in-situ observation of the solidification process of a

superalloy casting [3]. The movement of the grains, either upward or downward, depends on the balance between the liquid drag and the gravitational force acting on the grains. The further solidification or melting of the grains is determined by the local thermodynamic conditions. The mass transfer rate from the liquid to the equiaxed ($M_{\ell e}$) is shown in Fig. 2.3(e). Because $M_{\ell e}$ is proportional to n_e , a large value of $M_{\ell e}$ can be seen at the location where n_e is also large. The blue area in Fig. 2.3(e) implies that grain remelting also happened during the solidification process. Based on the simulation results, remelting was much weaker than solidification, and remelting only occurred occasionally. The calculated volume fraction of spurious grains (f_s) is presented in Fig. 2.3 (f). Spurious grains are intermittently distributed within the segregation channels. These simulation results have been validated through a directional solidification experiment. Comparison between the predicted freckles and the experimental measurements refers to [5].

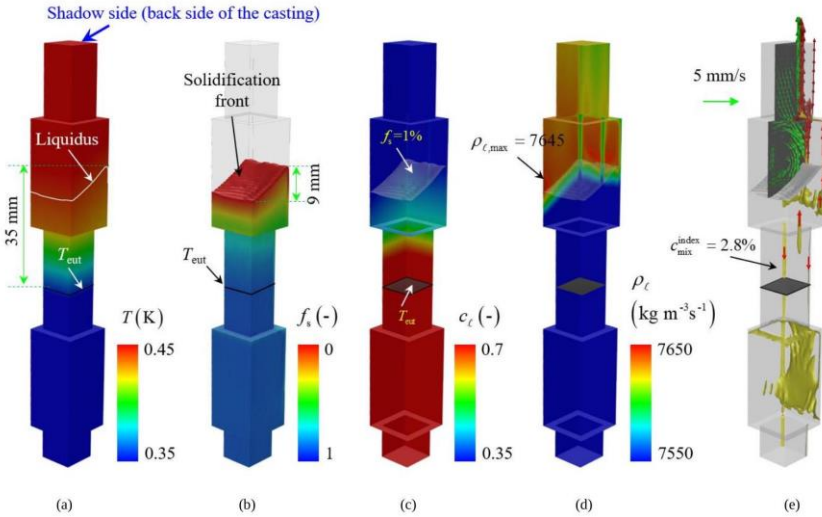


Fig. 2.2. Simulation results at 3800 s. (a) Temperature field T on the surface of the casing, overlaid by the liquidus and eutectic isotherms. (b) Solid fraction f_s and the shape of the solidification front. (c) Liquid concentration c_ℓ on the back and right walls of the casting, overlaid by the isosurfaces of $f_s = 1\%$ and $T = T_{eut}$. (d) Liquid density ρ_ℓ on the back and right walls of the casting; the maximal $\rho_{\ell,max} = 7645 \text{ kg m}^{-3} \text{ s}^{-1}$ is marked by the red lines. (e) The casting is rendered in transparent to show the plumes/channels indicated by the isosurfaces of $c_{mix}^{index} = 2.8\%$; the liquid flow in the plumes/channels is shown by the red vectors, and the liquid flow on a vertical section in the bulk liquid is shown by the green vectors.

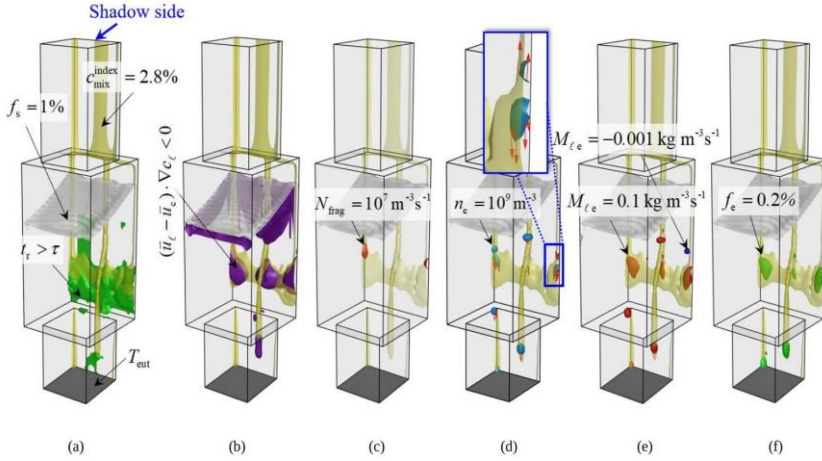


Fig. 2.3. Analysis of the formation of spurious grains at 4000 s. The casting is set to transparent to display the inside phenomena. The solidification front is indicated by the grey-inclined isosurface of $f_s = 1\%$, and the segregation channels are presented by the yellow isosurfaces of $c_{\text{mix}}^{\text{index}} = 2.8\%$. The bottom of the pictures coincides with the eutectic isotherm T_{eut} . (a) The region where the criterion $t_r > \tau$ is met is marked in green. (b) The region where the criterion $(\vec{u}_\ell - \vec{u}_c) \nabla c_\ell < 0$ is met is marked in purple. (c) Production rate of fragments N_{frag} , red isosurface of $N_{\text{frag}} = 10^7 \text{ m}^{-3} \text{ s}^{-1}$. (d) Number density of produced spurious grains n_e , blue isosurface of $n_e = 10^9 \text{ m}^{-3}$. (e) Mass transfer rate from the liquid to the equiaxed $M_{\ell e}$, red isosurfaces of $M_{\ell e} = 0.1 \text{ kg m}^{-3} \text{ s}^{-1}$ denote the solidification of the grains, and the blue isosurface of $M_{\ell e} = -0.001 \text{ kg m}^{-3} \text{ s}^{-1}$ denotes remelting of grains. (f) The volume fraction of spurious grains f_e , green isosurfaces of $f_e = 0.2\%$.

2.3.3 Effect of the Timing Effecting of Pinch-OFF

In this section, a new simulation was conducted with the same settings as the one introduced in the last sections, except for the ignorance of the timing effect for pinch-off. The simulation results and a comparison to the experimental measurements are shown in Fig. 2.4. Fig. 2.4(a) presents the experimentally measured microstructure of the vertical section taken from the lower segment of the larger cross-section. The brown areas represent the primary dendrites, while the white regions indicate the presence of eutectics. The dark spots indicate the mis-orientated spurious grains. Two long freckles are identified at the corners of the shadow side.

The simulation results are shown in Figs. 2.4(b)-(g). Comparing Figs. 2.4(b) and (e), a similar shape and distribution of the segregation channels were predicted. However, the calculated volume fraction of spurious grains (f_e) is significantly different. When the timing effect is ignored, fragments can be produced once the criterion $(\vec{u}_\ell - \vec{u}_c) \cdot \nabla c_\ell < 0$ is satisfied. As depicted in Fig. 2.3(b), fragments are produced not only in the segregation channels but also around the entire perimeter of the casting beneath the solidification front. As a result, the volume fraction of grains is significantly overestimated. A high volume fraction of grains is predicted near the whole surface of the casting, Fig. 2.4(b) and (c), which is inconsistent with the experimental measurements. For the case considering the timing effect, as shown in Fig. 2.3(c), fragments are only produced within the segregation channels, where the two criteria are satisfied. As shown in Fig. 2.4(f) and (g), two freckles (channels that have entrapped some spurious grains), are formed at the two corners of the casting. These simulation results align closely with the experimental findings in Fig. 2.4(a). According to the current study, incorporating timing effects in the flow-driven fragmentation model is crucial for accurately predicting the quantity of spurious grains and freckles.

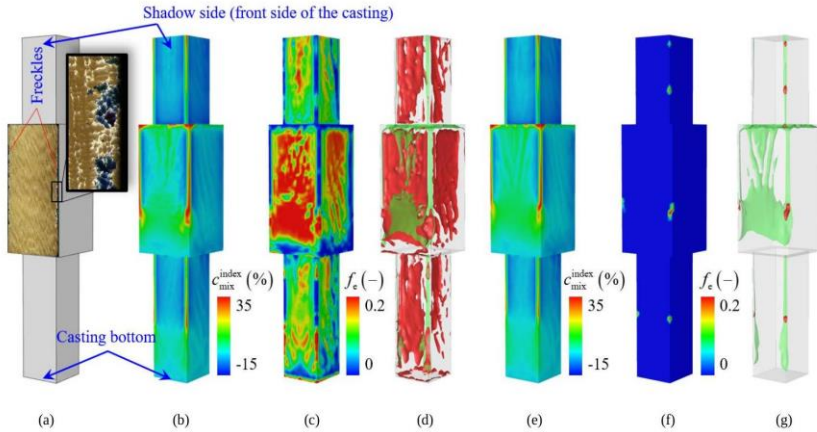


Fig. 2.4. Comparison study to highlight the necessity to consider the timing effect required for pinch-off before dendrite fragmentation. (a) The microstructure on the shadow side of the casting at the lower segment of the larger cross-section. (b)-(d) Simulation results ignoring the timing effect. (e)-(f) Simulation results considering timing effect. (b) and (e) Contour of the segregation index c_{mix}^{index} on the surface of the casting. (c) and (f) Contour of volume fraction of spurious grains f_e on the surface of the casting. (d) and (g) The casting is rendered transparent to show the distribution of freckles. The segregation channels are indicated by the green isosurfaces of $c_{mix}^{index} = 2.8\%$, and the spurious grains are indicated by the red isosurface of $f_e = 1\%$.

One may note in Fig. 2.4(g) that segregation channels form at both corners as well as in the region between them. However, spurious grains are only predicted within the two segregation channels at the casting corners, while the channels in the middle region remain free of spurious grains. The upward flow of the solute-enriched liquid is responsible for the onset of segregation channels, and the segregation channels are, somehow, inevitable during the directional solidification of the current superalloy. Spurious grain is produced when the melting conditions within these channels persist long enough to fragment dendrite side arms [12]. The strength of the upward flow in the relatively short channels (in the middle region) is much weaker than that in the two dominated channels at the casting corners, and some short channels vanish during the solidification process. Although segregation channels are developed there, the melting time is insufficient to pinch off the side arms and produce fragments, which explains the absence of freckles in the central region in the experimental and calculated results. These findings provide strong evidence for the timing effect required for pinch-off before dendrite fragmentation.

2.4 CONCLUSION

The directional solidification of a single-crystal superalloy sample with cross-sectional change is numerically studied by a previously proposed digital twin approach. The dendrite fragmentation is considered the sole source for spurious grains, and the timing effect required for pinch-off before dendrite fragmentation is considered. An improved simulation-experiment agreement in terms of both the distribution of segregation channels and spurious grains is achieved.

The shadow side of the casting is the most favourable position for the formation of freckles. The density inversion caused by the solute enrichment in the mushy zone leads to the onset of segregation channels. The upwelling flow within the channels promotes the melting of side arms. During this melting process, the timing effect plays a significant role in the formation of fragments. The roots of side arms will be pinched off and fragments are produced only when the local melting time is sufficiently long. Some channels shall be free of spurious grains due to insufficient melting time.

This study also demonstrates the difference between a segregation channel and a freckle. During the upward solidification of superalloy castings with density inversion (i.e., the solute-enriched liquid is less dense than the bulk liquid), the formation of segregation channels is almost inevitable. Spurious grains are generated after the channels have been well developed and only form in the channels where the melting condition persists for a sufficient duration. A segregation channel can be called a freckle only when it captures some spurious grains.

CONFERENCE DISCLAIMER

Abstract part of this manuscript was previously presented at the conference: The 8th International Conference on Solidification and Gravity dated from 2ed

September to 5th September 2024 in Miskolc - Lillafüred, Hungary, Web Link of the proceeding: <https://www.solgrav.uni-miskolc.hu/SG24-Program&Abstracts.pdf>

DISCLAIMER (ARTIFICIAL INTELLIGENCE)

Author(s) hereby declare that NO generative AI technologies such as Large Language Models (ChatGPT, COPILOT, etc.) and text-to-image generators have been used during the writing or editing of this manuscript.

ACKNOWLEDGEMENTS

This work was financially supported by the Austrian Science Fund in the framework of the FWF-NKFİN joint project (FWF, I4278-N36).

COMPETING INTERESTS

Authors have declared that no competing interests exist.

REFERENCES

1. Giamei AF, Kear BH. On the nature of freckles in nickel base superalloys, *Metall. Trans.* 1970;1:21852192.
2. Hellawell A, Sarazin JR, Steube RS. Channel convection in partly solidified systems, *Philos. Trans. - R. Soc. London, A.* 1993;345:507-544.
3. Reinhart G, Grange D, Abou-Khalil L, Mangelinck-Noël N, Niane NT, Maguin V, Guillemot G, Gandin CA, Nguyen-Thi H. Impact of solute flow during directional solidification of a Ni-based alloy: In-situ and real-time X-radiography, *Acta Mater.* 2020;194:68-79.
4. Pollock TM, Murphy WH. The breakdown of single-crystal solidification in high refractory nickel-base alloys, *Metall. Mater. Trans. A.* 1996;27:1081-1094.
5. Zhang H, Zhao Y, Xiong W, Ma D, Ludwig A, Kharicha A, Wu M. Modelling freckles and spurious grain formation in directionally solidified superalloy castings, *Commun. Mater.* 2024;5:232.
6. Zhang H, Liu X, Ma D, Song M, Ludwig A, Kharicha A, Wu M. Digital twin for directional solidification of a single-crystal turbine blade, *Acta Mater.* 2023;244:118579.
7. Zheng Y, Wu M, Kharicha A, Ludwig A. Incorporation of fragmentation into a volume average solidification model, *Model. Simul. Mater. Sci. Eng.* 2018;26:015004.
8. Zhang H, Wu M, Liu X, Ma D, Song M, Ludwig A, Kharicha A. Numerical study on the formation of spurious grains and freckles during the directional solidification of superalloys, *IOP Conf. Ser. Mater. Sci. Eng.* 2023;1281:012059.
9. Wu M, Ludwig A, Kharicha A. Volume-averaged modeling of multiphase flow phenomena during alloy solidification, *Metals (Basel).* 2019;9:229.
10. Zhang Z, Wu M, Zhang H, Hahn S, Wimmer F, Ludwig A, Kharicha A. Modeling of the as-cast structure and macrosegregation in the continuous

- casting of a steel billet: Effect of M-EMS, J. Mater. Process. Technol. 2022;301:117434.
11. Zhang H, Wu M, Rodrigues CMG, Ludwig A, Kharicha A, Rónaföldi A, Roósz A, Veres Z, Svéda M. Dendrite fragmentation mechanism under forced convection condition by rotating magnetic field during unidirectional solidification of AlSi7 alloy, Acta Mater. 2022;241:118391.
 12. Aagesen LK, Johnson AE, Fife JL, Voorhees PW, Miksis MJ, Poulsen SO, Lauridsen EM, Marone F, Stampanoni M. Universality and self-similarity in pinch-off of rods by bulk diffusion, Nat. Phys. 2010;6:796800.

Disclaimer/Publisher's Note: The statements, opinions and data contained in all publications are solely those of the individual author(s) and contributor(s) and not of the publisher and/or the editor(s). This publisher and/or the editor(s) disclaim responsibility for any injury to people or property resulting from any ideas, methods, instructions or products referred to in the content.

© Copyright (2025): Author(s). The licensee is the publisher (BP International).

Peer-Review History:

This chapter was reviewed by following the Advanced Open Peer Review policy. This chapter was thoroughly checked to prevent plagiarism. As per editorial policy, a minimum of two peer-reviewers reviewed the manuscript. After review and revision of the manuscript, the Book Editor approved the manuscript for final publication. Peer review comments, comments of the editor(s), etc. are available here: <https://peerreviewarchive.com/review-history/3590.2>